Naval Research Laboratory
Washington, DC 20375-5320

NRL/5670/MR—2023/3

Closeout Memorandum for Base Program 1V14: Phase-based Optical Frequency Receiver using Highly Dispersive Media

HANNAH M. OGDEN

ASEE Postdoctoral Fellow
Washington, DC

BRANDON REDDING

JOSEPH B. MURRAY

MATTHEW J. MURRAY

Optical Techniques Branch
Optical Sciences Division

October 27, 2023

REPORT DOCUMENTATION PAGE

Form Approved
OMB No. 0704-0188

1. REPORT DATE *(DD-MM-YYYY)*	**2. REPORT TYPE**	**3. DATES COVERED** *(From - To)*
27-10-2023	NRL Memorandum Report	10/1/20 – 9/30/23

4. TITLE AND SUBTITLE

Closeout Memorandum for Base Program 1V14: Phase-based Optical Frequency Receiver using Highly Dispersive Media

5a. CONTRACT NUMBER

5b. GRANT NUMBER

5c. PROGRAM ELEMENT NUMBER
0601153N

6. AUTHOR(S)

Brandon Redding, Hannah M. Ogden*, Joseph B. Murray, and Matthew J. Murray

5d. PROJECT NUMBER

5e. TASK NUMBER
EL-1153-104

5f. WORK UNIT NUMBER
1V14

7. PERFORMING ORGANIZATION NAME(S) AND ADDRESS(ES)

Naval Research Laboratory
4555 Overlook Avenue, SW
Washington, DC 20375-5320

8. PERFORMING ORGANIZATION REPORT NUMBER

NRL/5670/MR--2023/3

9. SPONSORING / MONITORING AGENCY NAME(S) AND ADDRESS(ES)

Naval Research Laboratory
4555 Overlook Avenue, SW
Washington, DC 20375-5320

10. SPONSOR / MONITOR'S ACRONYM(S)
NRL

11. SPONSOR / MONITOR'S REPORT NUMBER(S)

12. DISTRIBUTION / AVAILABILITY STATEMENT

DISTRIBUTION STATEMENT A: Approved for public release; distribution is unlimited.

13. SUPPLEMENTARY NOTES

*ASEE Postdoctoral Fellow, Optical Sciences Division, NRL Code 5674

14. ABSTRACT

This document satisfies the closeout requirements for NRL base program 1V14: Phase-based Optical Frequency Receiver using Highly Dispersive Media. It provides an overview of the technical objectives of the program, progress, and dissemination of research findings.

15. SUBJECT TERMS

Optical frequency
Frequency receiver
Brillouin scattering
Dispersive material
Heterodyne

16. SECURITY CLASSIFICATION OF:			**17. LIMITATION OF ABSTRACT**	**18. NUMBER OF PAGES**	**19a. NAME OF RESPONSIBLE PERSON**
					Matthew Murray
a. REPORT	**b. ABSTRACT**	**c. THIS PAGE**	U	13	**19b. TELEPHONE NUMBER** *(include area code)*
U	U	U			(203) 313-6624

This page intentionally left blank.

EXECUTIVE SUMMARY

This document satisfies the closeout requirements for NRL base program 1V14: Phase-based Optical Frequency Receiver using Highly Dispersive Media. It provides an overview of the technical objectives of the program, progress, and dissemination of research findings.

This page intentionally left blank.

CLOSEOUT MEMORANDUM FOR NRL BASE PROGRAM 1V14: PHASE-BASED OPTICAL FREQUENCY RECEIVER USING HIGHLY DISPERSIVE MEDIA

PROGRAM DESCRIPTION

The purpose of this program is to develop techniques to provide high resolution frequency measurements of short optical pulses. Many sensing technologies rely on measuring an optical frequency, such as spectroscopy, fiber sensors, LIDAR, and vibrometry. Enhanced measurements of optical frequencies could enable new sensors that could be used for battlespace awareness. For example, a fiber optic sensor with sufficient spatial resolution to operate as a distributed atmospheric acoustic sensor could be used for wide area unmanned aerial systems (UAS) detection.

Typically, applications requiring precise measurements of optical frequency rely on heterodyne detection and the resolution is driven by a mathematical limit known as the Cramer-Rao Lower Bound (CRLB). The CRLB-limited frequency resolution has a $\tau^{-3/2}$ dependence. This dependence on the pulse duration makes heterodyne detection schemes poorly suited for frequency measurements of short pulses. In this effort, we investigated a dispersive frequency receiver design with a different dependence on the pulse duration, in this case $\tau^{-1/2}$. This new approach has the potential to provide orders of magnitude higher frequency resolution in the short pulse regime.

TECHNICAL APPROACH

The dispersive frequency receiver operates by mapping changes in frequency to a change in phase. This mapping is achieved using a dispersive material, which is defined as a material with a refractive index that changes as a function of optical frequency. The dispersion is the slope of the refractive index as it changes with frequency. The larger this dispersion, the more efficient this mapping from frequency to phase.

Light passing through a dispersive material accumulates a frequency-dependent phase delay with a slope of:

$$\frac{d\phi}{df} = k\,L\,\frac{dn}{df} \tag{1}$$

where k is the wavenumber and $k = 2\pi/\lambda$, L is the length of the dispersive material, and $\frac{dn}{df}$ is the material dispersion. To use this dispersive response to measure optical frequency, we can construct an interferometer with a dispersive material in one arm. By measuring the relative phase between the two arms of the interferometer, we can recover the optical frequency (after calibrating the interferometer at a known frequency). In particular, the frequency of an unknown signal under test (SUT), f_{SUT}, can be obtained as:

$$f_{SUT} = f_{cal} - \frac{\Delta\phi_{meas}}{k\,L\,(dn/df)} \tag{2}$$

where $\Delta\phi_{meas}$ is the change in measured phase relative to the phase measured at the calibration frequency, f_{cal}. To estimate the frequency uncertainty of this type of system, we first calculate the uncertainty in the measured phase as

$$\sigma_\phi = \frac{1}{\sqrt{2CNR}} \tag{3}$$

Manuscript approved October 26, 2023.

where CNR is the carrier-to-noise ratio. Assuming shot-noise-limited detection, the CNR can be expressed as:

$$CNR = \frac{m\eta\, P_{pk}\tau_{pulse}}{h\nu} \tag{4}$$

where m is the mixing ratio, η is the detector efficiency, P_{pk} is the optical peak power of the signal under test, τ_{pulse} is the duration of the pulse, h is Plank's constant, and ν is the frequency of light. Therefore, the uncertainty in the frequency is

$$\sigma_f = \frac{\sqrt{h\nu}}{\sqrt{2}k\, L \left|\frac{dn}{df}\right| \sqrt{m\eta\, P_{pk}\tau_{pulse}}} \tag{5}$$

where we have used Eq. (2) to convert to frequency.

On the other hand, for heterodyne-based frequency receivers, the frequency resolution is given by the CRLB:

$$\sigma_{f,CRLB} = \frac{\sqrt{6}}{2\pi\tau_{pulse}\sqrt{CNR}}. \tag{6}$$

Again, assuming shot-noise-limited detector, the frequency uncertainty can be expressed as:

$$\sigma_{f,CRLB} = \frac{\sqrt{6h\nu}}{2\pi\tau_{pulse}\sqrt{m\eta\, P_{pk}\tau_{pulse}}}, \tag{7}$$

illustrating the $\tau^{-3/2}$ dependence. This dependence on the pulse duration makes heterodyne detection schemes poorly suited for frequency measurements of short pulses. Figure 1 shows the expected frequency resolution for the CRLB-limited heterodyne receiver as well as the resolution for the dispersive receiver with various magnitudes of dispersion.

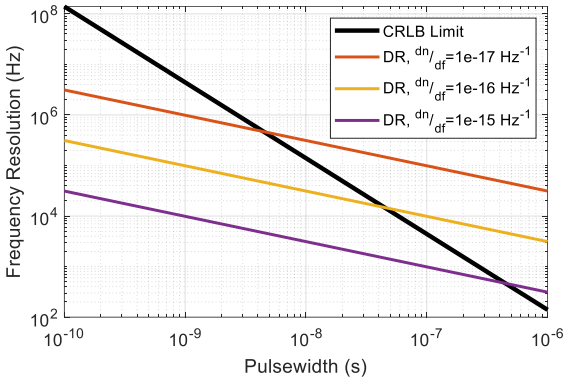

Figure 1. Expected frequency resolution of the CRLB-limited heterodyne approach as well as the expected resolution for the dispersive receiver (DR) with dispersion magnitudes of $dn/df = 1e-17, 1e-16$, and $1e-15$ Hz^{-1}.

In order to tailor the dispersive properties of a material we have taken advantage of Stimulated Brillouin Scattering (SBS) in optical fiber to generate dispersion. In stimulated Brillouin scattering a high-power pump beam and a counter-propagating probe beam are launched in an optical fiber. The two beams interact with one another and through electrostriction generate an acoustic wave. The frequency of the acoustic wave, which is called the Brillouin frequency, is set by the material properties and the frequency of the optical pump. If the frequency separation between the pump and probe beam is equal to the Brillouin frequency, then the probe beam will experience gain as energy is transferred from the pump beam. By scanning the frequency of the probe beam, it is possible to map out the gain spectrum, which typically has linewidth of ~30 MHz in optical fiber.

Our technique relies on generating a pair of closely spaced (< 200 MHz) Brillouin gain features. Light with a frequency in between the gain features will experience dispersion with negligible gain/absorption. The advantage of this technique is that the frequency region over which the dispersion is constant is easily tunable by controlling the frequency separation between two pump beams. Another advantage of this

technique is that standard commercial off-the-shelf fiber can be used to generate the dispersion and the fiber can easily provide interaction lengths of 100 – 500 m (note the factor of L in Eq. (5)).

PHASE-BASED DISPERSIVE FREQUENCY RECEIEVER

Conventionally, Brillouin-based frequency measurements (so-called Brillouin optical spectrum analyzers (BOSA)) operate by scanning a pump beam and measuring the resulting Brillouin amplification across a frequency band of interest. However, this technique is time-consuming, which prohibits dynamic measurements. Additionally, this approach makes it challenging to achieve a spectral resolution better than the Brillouin linewidth. This effort addresses both limitations.

The basic design of the dispersive frequency receiver is shown in Fig. 2(a). In this design two pump beams are generated by an electro-optic modulator (EOM) and an arbitrary waveform generator. The pumps are sent down an interaction fiber to generate a pair of Brillouin gain peaks separated from the pumps by the Brillouin frequency (f_B). The signal under test (SUT), which has a frequency that is in between the two gain peaks, counter propagates through the fiber where it experiences the dispersion induced by the gain peaks, but with minimal gain. The SUT is directed to a detector where the phase of the signal is measured with coherent detection (using a reference arm not shown) and Eq. (2) is used to recover f_{SUT} as:

$$f_{SUT} = f_{cal} - \frac{\Delta\phi_{meas}}{k\,L\,(dn/df)} = f_0 - f_B - \Delta f_{SUT} \tag{8}$$

where f_0 is the laser frequency and f_B is the Brillouin frequency of the fiber, and we use a calibration frequency of $f_{cal} = f_0 - f_B$. We also define Δf_{SUT} as the frequency difference between the SUT and the calibration frequency. Figure 2(b) shows a cartoon of the relevant optical frequencies, Brillouin gain spectrum G_B, and corresponding change in refractive index Δn.

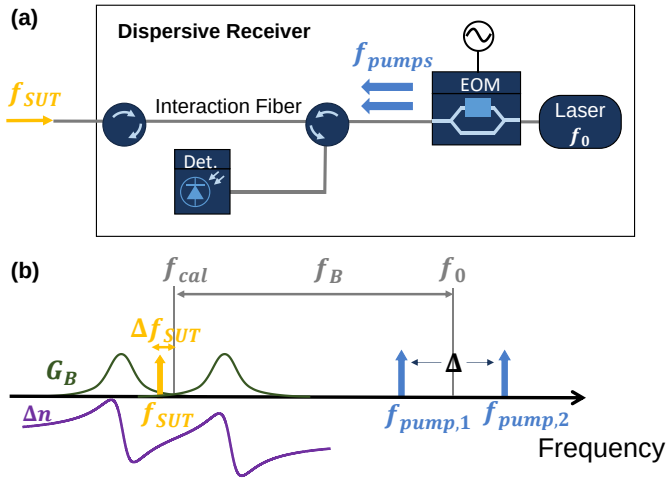

Figure 2. (a) Schematic of the basic dispersive frequency receiver design. (b) Diagram of the relevant frequencies involved with the dispersive frequency receiver.

Initially, we developed a model of the dual pump Brillouin system to evaluate the ideal separation between the two gain features. The complex gain spectrum from a single pump beam was modeled using the complex gain factor g (R. W. Boyd, *Nonlinear Optics*, (Academic Press, 2008)):

$$g(f) = \frac{\gamma_e^2\left(2\pi f_{pump}\right)\epsilon_0 f_B^2}{2nc\rho v_s^2} \frac{i}{i\left(f_{pump} - f\right)\Gamma_B - \left(f_B^2 - \left(f_{pump} - f\right)^2\right)} \tag{9}$$

where γ_e is the electrostriction coefficient, ϵ_0 is the permittivity of free space, n is the refractive index of the material, c is the speed of light, ρ is the material density, v_s is the sound velocity in the material, f_{pump} is the frequency of the pump beam, Γ_B is the Brillouin linewidth, and f is the optical frequency. The gain

factor for two pump beams is a direct sum of the individual gain factors: $g = g_1 + g_2$. The total complex gain is given by

$$\tilde{G} = g\, A_{pump}^2\, L = G_B + i\phi_B \tag{10}$$

where A_{pump} is the amplitude of the pump electric field, L is the interaction length, and G_B is the Brillouin gain and ϕ_B is the Brillouin phase. Note that the intensity of the pump beam is given by $I_{pump} = 2n\epsilon_0 c\left|A_{pump}\right|^2$. From Eq. (10) it is clear that the Brillouin phase $\phi_B = Im\{\tilde{G}\}$.
The change in refractive index is given by

$$\Delta n(f) = \frac{\phi_B\, c}{2\pi L(f + f_B)}. \tag{11}$$

The simulated refractive index from two pump beams was fit to a linear function over a frequency range between the two gain peaks over which the slope is approximately constant. The slope of the fit provided a simulated measure of the dispersion. Figure 3(a) and 3(b) shows an example of the simulated gain spectrum (i.e. $Re\{\tilde{G}\}$) and refractive index, respectively. The recovered dispersion magnitude for a range of frequency separations is shown in Fig. 4. For these simulations the magnitude of the gain was matched to the experimentally measured gain (0.64).

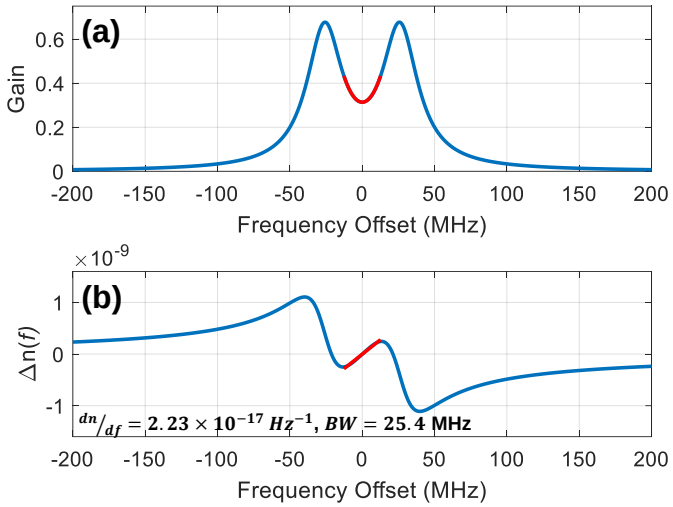

Figure 3. Simulated Brillouin gain curve (a) and corresponding refractive index (b) for two pump beams separated by 52 MHz. The linear portion of the refractive index is fit with a linear regression (red) to obtain the dispersion.

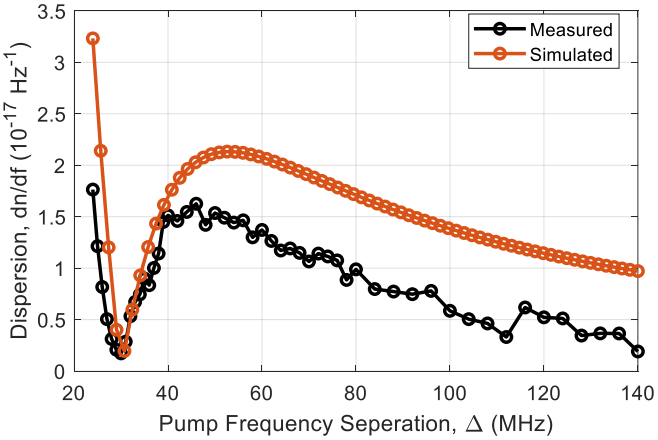

Figure 4. Comparison of simulated and experimentally measured dispersion,

The model was verified with experiments. For these experiments, a known frequency modulation was applied to the signal under test and the resulting phase was measured at a range of pump separations from 24 to 140 MHz. The dispersion was calculated using Eq. (2). Figure 4 shows the recovered dispersion at each frequency separation. Overall, the simulated and measured results are in good agreement. There is a discrepancy, especially at larger frequency separations, which could be a result of the presence of the local oscillator (used for coherent detection). While the model predicted that peak dispersion occurred at a frequency separation of 52 MHz, the experimentally measured peak occurred at 46 MHz. Using the experimentally measured peak allowed us to maximize the sensitivity of the dispersive receiver.

Using the optimized frequency separation of 46 MHz, we operated the dispersive receiver as a wavemeter. For this test, we measured a beam with a sinusoidal frequency modulation at 12 kHz with an amplitude of 500 kHz and recorded a 10 ms measurement of the phase of the light after it passed through the interaction fiber. We used the experimentally measured dispersion ($dn/df = 1.63 \times 10^{-17}$ Hz^{-1}) to convert the measured phase to frequency. An amplitude spectral density (ASD) of the recovered frequency is shown in Fig. 5. We measured a frequency noise of 670 Hz/√Hz. This is approximately four orders of magnitude below standard Brillouin-based frequency measurement systems, which are typically limited to the Brillouin linewidth (~30 MHz).

Ultimately, this was a successful demonstration of the dispersive frequency receiver design, however the system suffered from several limitations. First, the approach was particularly sensitive to both temperature fluctuations and laser frequency noise since both affect the frequencies of the Brillouin gain peaks. For example, in order to improve the system frequency noise, it would be necessary to stabilize the temperature of the interaction fiber to within 1 m^0C. Furthermore, the measurement was also sensitive to pump power fluctuations, which affects the gain and therefore the magnitude of the dispersion. Finally, the approach was also sensitive to out-of-band noise on the signal under test. As a result of these limitations, we developed a modified approach.

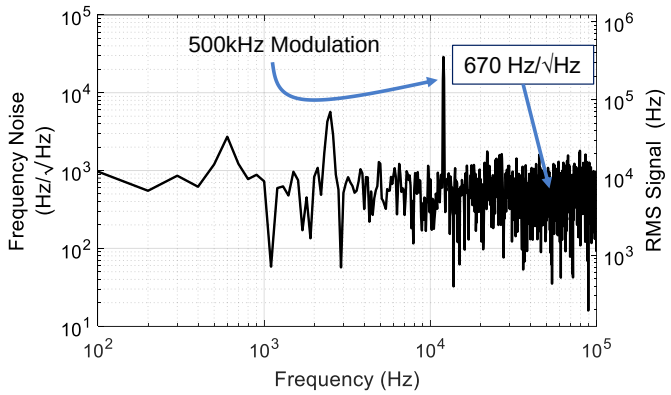

Figure 5. Amplitude spectral density of the measured frequency using the phase-based dispersive receiver. A peak at 12 kHz shows a frequency modulation with a magnitude of 500 kHz.

SLOPE-ASSISTED BRILLOUIN WAVEMETER

To address the limitations of the dispersive receiver, we built a second-generation system, which required several changes. First, rather than only measuring the phase of a single probe beam, we measured both the SBS-induced phase and gain. This allowed us to estimate the optical frequency using the phase-to-gain ratio, which has a linear frequency dependence regardless of the pump power. Second, we adjusted the experimental setup so that we could measure the phase-to-gain ratio from both the Stokes and anti-Stokes interactions. This allowed us to identify changes in the frequency of the SUT independent of the Brillouin frequency shift in the fiber, rendering the system immune to temperature and mechanical fluctuations. Third, rather than detecting the SUT directly, the SUT served as the pump and the frequency was estimated from two probe beams which interacted with the Stokes and anti-Stokes gain features. This

allowed the system to be insensitive to any out-of-band signals/noise in the SUT beam. This system is also capable of dynamic frequency measurements.

Using this improved apparatus, we demonstrated a frequency noise spectral density of 20 Hz/√Hz. We achieved a frequency resolution 2 orders of magnitude better than our first-generation system and 6 orders of magnitude below the Brillouin line width for a 10 ms measurement. Additionally, we experimentally verified that the sensor can operate over a frequency range of 40 MHz and is immune to temperature variations of as much as 5 °C. A journal article describing this work was published in *IEEE Photonics Technology Letters* in April 2022. A provisional patent for this work has also been filed and was approved by the IEB (Navy Case # 21112).

Although this approach achieved record-setting performance, the system had several limitations. First, the system had a narrow operating range of 40 MHz that was dictated by the Brillouin linewidth. Furthermore, the system operated as a wavemeter—meaning that it could only detect a single frequency at a time. Finally, this system was designed to measure the frequency of the SUT indirectly, through the Brillouin interaction with the probe beams. As a result, the length of the interaction fiber imposes a lower limit on the pulse duration that can be measured (in this case 5 µs for a 500 m interaction fiber). Therefore, this system was not well-suited to measuring the frequency of pulsed light.

UPDATED FREQUENCY RECEIEVER DESIGN AND ANALYSIS

Based on the information that was learned from the first dispersive receiver and the Brillouin wavemeter, we developed an updated dispersive frequency receiver design. In this approach, similar to the first dispersive frequency receiver, the SUT was detected directly, which enabled frequency measurements of short optical pulses. Figure 6(a) shows a schematic of the design and Fig. 6(b) shows a diagram of the relevant frequencies. A key aspect of this design is that (similar to the Brillouin wavemeter) it uses information from both the Stokes and anti-Stokes Brillouin peaks to compensate for environmental perturbations (temperature and mechanical stress).

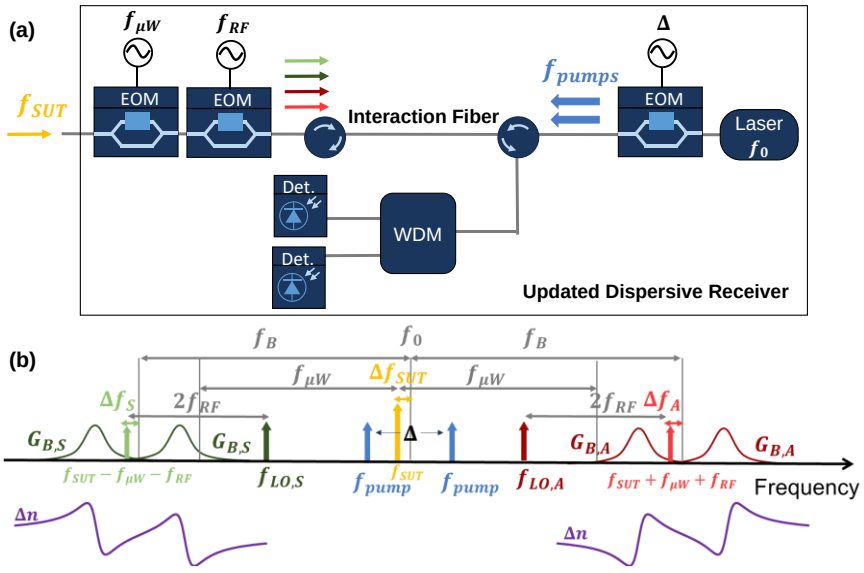

Figure 6. (a) Updated dispersive frequency receiver design using information from both the Stokes and anti-Stokes Brillouin peaks. (b) Frequency diagram for the updated design.

As before, a pair of pump beams are sent down an optical fiber to generate a pair of Brillouin peaks. The signal under test, which has a frequency that is in between the two pump frequencies, is split into four beams using a pair of EOMs. One beam lies in between the two Stokes peaks and another lies in between the two anti-Stokes peaks. In addition, a pair of co-propagating local oscillators (LOs, $f_{LO,S}$ and $f_{LO,A}$) allow the system to measure the Brillouin phase. The subscripts S and A denote Stokes and anti-Stokes,

respectively. The LOs are sufficiently shifted from the peaks so that there is minimal interaction between the Brillouin peaks and the LOs. The four beams counter-propagate through the optical fiber and are detected using a pair of photodetectors. A wavelength division multiplexer (WDM) separates the Stokes and anti-Stokes frequencies. The beams that lie in between the Stokes peaks and anti-Stokes peaks each accumulate a phase as they propagate through the fiber. To compensate for environmental perturbations, the measured phase from the anti-Stokes beam is subtracted from the phase from the Stokes beam:

$$f_{SUT} = f_{cal} + \frac{\phi_{B,S} - \phi_{B,A}}{k\, L\, (dn/df)} \tag{12}$$

Here, $f_{cal} = f_0$. In this configuration, the frequency resolution of the dispersive receiver is given by

$$\sigma_f = \frac{\sqrt{h\nu}}{k\, L \left|\frac{dn}{df}\right| \sqrt{m\eta\, P_{pk} \tau_{pulse}}}. \tag{13}$$

This frequency resolution is a factor of $\sqrt{2}$ larger than the first-generation approach as a result of using two measurements of the phase. (Note that there is also a factor of 2 enhancement in the responsivity that is canceled out by the fact that the SUT is split into four beams.) It is important to note, that while this configuration enables measurements that are immune to temperature drifts or mechanical stress on the interaction fiber, it remains susceptible to frequency fluctuations of the laser.

We conducted an analysis of the expected performance of this frequency receiver design. We calculated the expected frequency uncertainty for the CRLB and the dispersive receiver using Eqns. (7) and (13). For these calculations the peak signal power was chosen to be 1 µW and both the mixing efficiency and detector efficiency were set to 1. The wavelength used in these calculations was 1549.32 nm. The maximum dispersion predicted in Fig. 4 occurs at a frequency separation of 52 MHz and has a value of 2.2×10^{-17} Hz^{-1}. The maximum predicted dispersion was used in estimating the expected frequency uncertainty of the dispersive receiver. Figure 7(a) shows the frequency uncertainty as a function of pulse duration for the CRLB (black line) and the dispersive receiver (colored lines). The dispersive receiver uncertainty is shown at four fiber lengths. For reference, the transform limit of the pulse is also shown on the plot. Somewhat surprisingly, both the CRLB and dispersive receiver outperform the transform limit, which is possible since both methods are able to centroid on the frequency of the SUT.

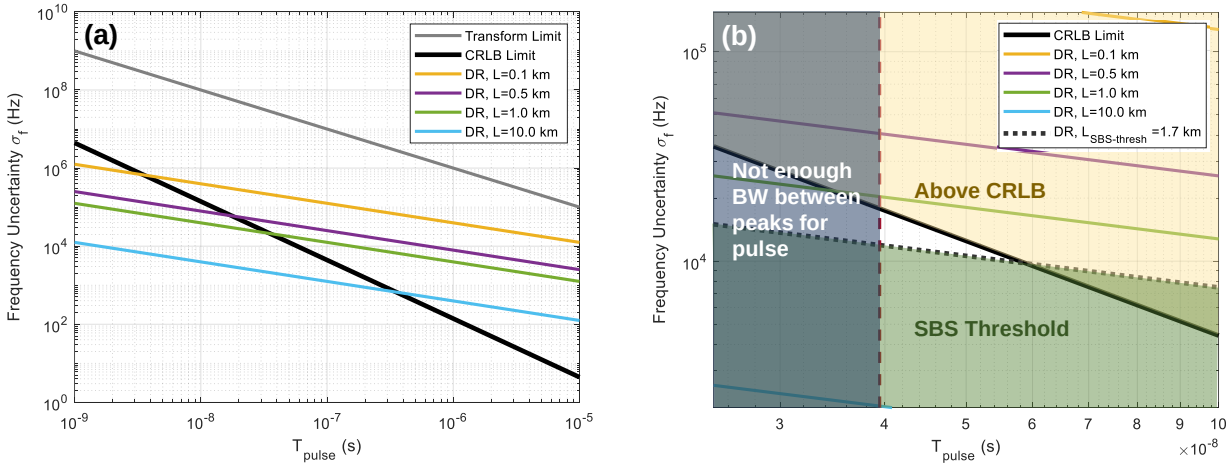

Figure 7 (a) Frequency uncertainty as a function of pulse duration based on the CRLB limit and the dispersive receiver (DR). The uncertainty for the DR is shown for several lengths of fiber. The calculations were based on 1 µW of received power, 25.5 mW of pump power, corresponding to dispersion of 2.2×10^{-17} Hz-1. Also shown on the plot is the transform limit of the pulse. (b) Zoomed in view of Fig. 7(a). The linear portion of the refractive index is 25 MHz, corresponding to a minimum pulse duration of 39 ns. At this power level, spontaneous Brillouin scattering is initiated using 1.7 km of fiber and represents an upper limit on the amount of fiber that can be used.

Figure 7(a) also illustrates the different pulse duration scaling of the CRLB and the dispersive receiver. At short pulses the dispersive receiver outperforms the CRLB. This plot suggests that for a sufficiently long interaction length and short enough pulse, it is possible to outperform the CRLB by several orders of magnitude. However, it is important to note that there needs to be sufficient bandwidth (frequency separation) between the two gain peaks for the transform limited pulse containing the signal under test. The pulse's spectrum must be contained within the linear portion of the refractive index so that it experiences a constant dispersion. This requirement sets a lower limit on the pulse duration used in this frequency measurement. For the simulation shown here, the linear portion of the refractive index spans 25.4 MHz (see Fig. 3), which corresponds to a minimum pulse duration of 39 ns. Pulses shorter than this value have a spectrum that exceed the width of the linear portion of the refractive index. As shown in Fig, 7(b) this drastically reduces the regions in the graph where the dispersive receiver outperforms the CRLB.

Finally, another important parameter to consider is the onset of spontaneous Brillouin scattering. At the high pump powers needed for these experiments, spontaneous Brillouin scattering and other nonlinear phenomena can limit the ability of the coherent receiver to accurately recover the phase. The spontaneous Brillouin scattering threshold places an upper limit on the length of fiber used for the measurement. As shown in Fig. 7(b) this final constraint eliminates nearly all configurations that can outperform the CRLB. Only lengths between 1.1 km and 1.7 km have the ability to outperform the CRLB at this power level and frequency separation. This analysis indicates that the dispersive receiver design has the potential to outperform the CRLB by a factor of ~1.6 after accounting for limitations on the pulse duration and the spontaneous Brillouin threshold.

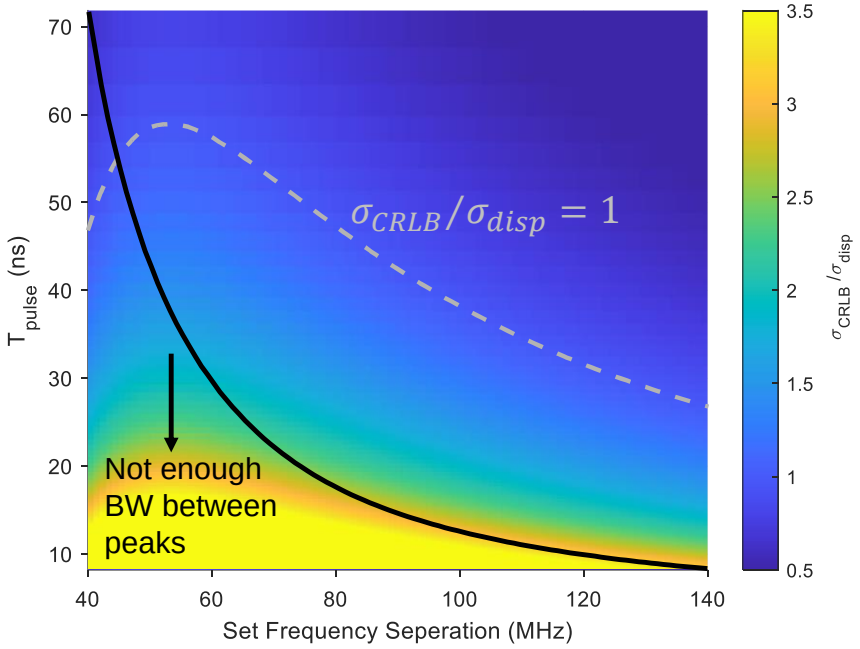

Figure 8. Design space analysis showing the possible frequency resolution improvement with the dispersive receiver over the CRLB for various pulse durations and pump frequency separations. Also shown on the plot is a black line which represents the minimum pulse duration that can be used for a given frequency separation. The area below this line represents configurations where the pulse spectrum exceeds the linear portion of the refractive index. The gray dashed line shows where the frequency resolution of the dispersive receiver matches the CRLB.

It is possible to consider other configurations that may offer better performance. To evaluate the configurations that have the best chance at outperforming the CRLB, we assume that we operate right at the spontaneous scattering threshold as this offers the best chance to improve performance. It is important to note that given this assumption, the product $L\left|\frac{dn}{df}\right|$ in Eq. (13) only depends on the frequency separation and is independent of the set fiber length and power level. Therefore, this assumption allows us to remove

fiber length and power level from our design space analysis. Figure 8 shows a contour plot of the ratio of the frequency resolution of the CRLB to the frequency resolution of the dispersive receiver $\sigma_{CRLB}/\sigma_{disp}$ on a grid of pulse durations and frequency separations. The gray dashed line represents the point where the CRLB and dispersive receiver have the same resolution. Also shown on the plot is a black line which represents the minimum pulse duration that can be used for a given frequency separation. The area below this line represents configurations where there the pulse spectrum exceeds the linear portion of the refractive index and should not be used for frequency measurements. The area in between the gray dashed line and the black line represents configurations where the dispersive receiver can outperform the CRLB. From the plot it is clear the pulse duration limitation imposed by the frequency separation severely reduces the configurations that have the greatest potential to outperform the CRLB. It is also evident that moving to a larger frequency separation, actually benefits the performance compared to the CRLB measurement since a shorter pulse duration can be used. This analysis shows that with this design it is possible to outperform the CRLB by a factor of ~3.

In summary, the dispersive receiver operates by mapping a change in frequency to a change in phase. In the design presented here, this transfer is accomplished using a pair of Brillouin gain peaks. In between the gain peaks the refractive index changes linearly with frequency and the slope of this changing refractive index is known as the dispersion. The larger the dispersion, the more responsive phase is to a change in frequency. In this program we have modeled the Brillouin-scattering-induced dispersion and validated the model with experimental measurements, developed a frequency uncertainty model, and analyzed the design space for our Brillouin-scattering-based receiver. Our analysis includes constraints imposed by the transform limit of the pulse and the non-linear spontaneous Brillouin scattering threshold of the fiber.

The dispersive receiver design presented here offers a path to outperform the CRLB, however, this improvement is relatively modest. The frequency resolution improvement is limited by the frequency range over which the refractive index is linear and the spontaneous scattering threshold. Although our analysis showed that the Brillouin scattering design offers only modest improvement over the CRLB, the framework presented here could be used to analyze other dispersive frequency receiver designs with different dispersive materials in the future.

FREQUENCY SHIFTING LOOP SPECTROMETER

One of the main limitations of the frequency receiver systems presented here is the limited range over which they operate. One way to address this limitation is by tuning the pump laser (in the case of the dispersive receivers) or the probe laser (in the case of the Brillouin wavemeter) so that the system has an expanded range. This tuning could be achieved using a tunable laser or a single sideband modulator. However, achieving high-speed linear frequency tuning over a wide range is a long-standing challenge. As a way to investigate alternate approaches to linear wideband frequency tuning, we developed an approach using frequency shifting fiber loops and used that approach to make a high-speed broadband absorption spectrometer.

Frequency shifting loops (FSLs) contain a fiber optic ring cavity with a frequency-shifting modulator, an amplifier to compensate for loss, and a filter to suppress amplified spontaneous emission (ASE). With each trip around the loop the light accumulates a discrete frequency shift. Although, FSLs have been used for a variety of applications, they typically have a limited bandwidth due to the accumulation of ASE. We developed an approach using a pair of cascaded FSLs to dramatically increase the bandwidth of FSL architectures. We showed using a pair of cascaded FSLs, we could produce 2000 pulses that span 200 GHz in 100 MHz steps. Our analysis indicated that with proper components, this technique could enable high-speed scanning over 1 THz in 10,000 frequency steps. As an example application, we showed that this technique could be used to monitor the absorption spectrum of HCN gas. A journal article describing this work was published in *Scientific Reports* in April 2023.

BRILLOUIN LASER SPECTROMETER

To greatly improve the operating range of frequency detection and to enable detection of more than one optical frequency at once, we also developed a Brillouin-laser-based spectrum analyzer. The technique leverages the wavelength dependence of the Brillouin frequency shift to compress a 4 THz (25 nm) wide optical spectrum in the C-band into a 230 MHz radio frequency (RF) spectrum. The unknown optical spectrum is sent into a fiber ring cavity where it acts an optical pump exciting frequency-shifted Brillouin laser modes. A copy of the original optical spectrum is sent to a detector where it interferes with the Brillouin-shifted lasing modes, producing a spectrum in the RF domain. The RF spectrum is recorded with a standard analog-to-digital converter, providing high-speed detection. The self-referenced approach removes the need for a tunable laser (as is required in both existing BOSA and heterodyne-based frequency receivers) and the narrow linewidth lasing modes facilitate measurement of Brillouin frequency shifts well below the Brillouin linewidth. The Brillouin laser spectrometer can continuously monitor a 4 THz wide optical spectrum with 28 MHz resolution using a 5 ms acquisition time. Additionally, the system can detect multiple lines with a minimum resolvable separation of 8 GHz and a dynamic range of 15 dB. This provided a simple approach to high-resolution, broadband spectral analysis (albeit with lower resolution than the slope-assisted Brillouin wavemeter we developed earlier in this effort). This work was published in *APL Photonics* in July 2023. A patent for this work has also been filed with the U.S. Patent and Trade Office, App No. 18/243,728 (Navy Case # 211313).

DISSEMINATION

Peer Reviewed Journal Articles

1. M. J. Murray, J. B. Murray, and B. Redding, "Slope-Assisted Brillouin Optical Wavemeter," IEEE Photonics Technol. Lett. **34**(9), 479–482 (2022).
2. H. M. Ogden, J. B. Murray, M. J. Murray, and B. Redding, "High-speed broadband absorption spectroscopy enabled by cascaded frequency shifting loops," Sci. Rep. **13**, 5762 (2023).
3. J. B. Murray, M. J. Murray, and B. Redding, "Brillouin laser spectrometer based on spectral compression," APL Photonics **8**, 76106 (2023).

Patents

1. J. B. Murray, B. Redding, M. J. Murray, “Brillouin fiber laser spectrometer”, Application No. 18/243,728, Navy Case #: 211313.
2. M. J. Murray, J. B. Murray, B. Redding, “Brillouin Wavemeter” Provisional Application No. 63/368,716, Navy Case #: 211121.

Conference Presentations

1. B. Redding, J. B. Murray, and M. J. Murray, "Using Brillouin scattering in optical fiber for sensing, spectroscopy, and optical signal processing," in Proc. SPIE 12532, *Optical Waveguide and Laser Sensors II*, 1253206 (15 June 2023).
2. J. B. Murray, M. J. Murray, and B. Redding, "Optical spectrum analyzer based on pulsed Brillouin lasing," in Proc. SPIE 12516, *Next-Generation Spectroscopic Technologies XV*, 125160P (15 June 2023).